ARTICLE

Controlling Liquid Crystal Alignment Using Photocleavable Cyanobiphenyl Self-Assembled Monolayers

Panida Prompinit,[†] Ammathnadu S. Achalkumar,[‡] Jonathan P. Bramble,[†] Richard J. Bushby,[‡] Christoph Wälti,[§] and Stephen D. Evans*[,†]

Molecular and Nanoscale Physics, School of Physics and Astronomy, Centre for Molecular Nanoscience (CMNS), and Institute of Microwaves and Photonics, School of Electronic and Electrical Engineering, University of Leeds, Leeds LS2 9JT, United Kingdom

ABSTRACT We report on the development of novel cyano-biphenyl-based thiolate self-assembled monolayers designed to promote homeotropic alignment of calamitic liquid crystals. The molecules developed contain an *ortho*-nitrobenzyl protected carboxylic acid group that on irradiation by soft UV (365 nm) is cleaved to yield carboxylic acid groups exposed at the surface that promote planar alignment. Using a combination of wetting, X-ray photoelectron spectroscopy, Fourier transform-infrared reflection absorption spectroscopy, and ellipsometry we show that high photolysis yields (>90%) can be achieved and that the patterned SAMs are suitable for the controlled alignment of calamitic liquid crystals. This study further shows that such photo-patterned SAMs can be used to control the formation of focal conic domains (FCDs) in the smectic-A phase in terms of positioning and size confinement on surfaces.

KEYWORDS: self-assembled monolayers • *ortho*-nitrobenzyl • liquid crystal • patterned surface • focal conic domains (FCDs)

1. INTRODUCTION

Liquid crystals (LCs) are increasingly finding application, beyond their commercial role in display devices (1−3), in the areas of chemical and biological sensing (4−7) and photonic devices (8−10). An important parameter for their application is the ability to control their alignment at interfaces. There are various methods used for LC alignment, such as rubbed or photoaligned polymer films (11, 12), evaporated oxides (13), and self-assembled monolayers (SAMs) (14−16). The application of SAMs opens new opportunities because of the ease with which they can be patterned, with nanometer resolution and over macroscopic areas. LC anchoring can be readily controlled by varying the functionality of the terminal from high energy, polar, surfaces such as carboxylic acid (−COOH) (15, 17, 18) or hydroxyl (−OH) (15, 18−20) to low energy methyl ($-CH_3$) (14, 15, 20) or perfluorocarbon ($-CF_3$) (19, 21). Additionally, it is also possible to display "LC-like" groups, such as cyano biphephenyl and terphenyl derivatives at the SAM surface (22−27). Such LC analogues have been shown to be useful in controlling the alignment in an overlying LC phase, dependent on the orientation of LC SAM (22). Further, the use of micropatterning of such SAMs can provide additional control over the azimuthal alignment (16, 28−30). Current patterning techniques are microcontact printing (μCP) (15, 16, 29) and photolithography (19, 31). Most soft UV methods are based on the photodeprotection of *ortho*-nitrobenzyl derivatives generating a hydroxyl (32), amine (33, 34), or carboxylic acid group at the surface (35−37). Recently, we have reported a high photodeprotection yield of *ortho*-nitrobenzyl (>90%) using an acid catalyst solution overlayer which led to high quality patterned SAMs (37).

In this paper, we describe a novel LC-based SAM (**SAM1**), suitable for the functionalization of gold surfaces, Figure 1. The SAM forming molecules (reagent **1**) contain a cyanobiphenyl unit oriented to promote homeotropic alignment in an overlying LC phase. Upon irradiation with soft UV (365 nm), cleavage at the *ortho*-nitrobenzyl site occurs with greater than 90% efficiency to leave a carboxylic acid functionalized surface (**SAM2**) (37). Such photopatterned areas promote planar anchoring, and thus, the photopatterning provides contrasting regions of homeotropic and planar alignment. This is demonstrated using the calamitic liquid crystal 8-cyanobiphenyl (8CB).

2. EXPERIMENT METHODS

Materials. Dichloromethane (DCM, 99.9%), hydrogen peroxide (27.5 wt.%), 4,4′-dithiobutyric acid, $-[S(CH_2)_3\text{-}CO_2H]_2$ (DTBA), 1 M hydrochloric acid, and isopropyl alcohol (IPA, 99.9%) were used as received from Sigma-Aldrich. Sulfuric acid (98%) was supplied by Fisher Scientific. The nematic liquid crystal used in this study was 4-*n*-octyl-4-cyanobiphenyl (8CB, Merck). Glass microscope slides (thickness 0.8 mm) were purchased from Agar and were cut to approximately three-quarters of the original length. Millipore Milli-Q water with a resistivity better than 18.1 MΩ · cm was used throughout. High purity (99.99%) temper-annealed gold wire (0.75 mm diameter) was supplied by Goodfellow.

* Corresponding author. Phone: +44 113 343 3852. E-mail: s.d.evans@leeds.ac.uk.

Received for review September 3, 2010 and accepted October 26, 2010

[†] Molecular and Nanoscale Physics, School of Physics and Astronomy.

[‡] Centre for Molecular Nanoscience (CMNS).

[§] Institute of Microwaves and Photonics, School of Electronic and Electrical Engineering.

DOI: 10.1021/am100832p

Published on Web 11/11/2010

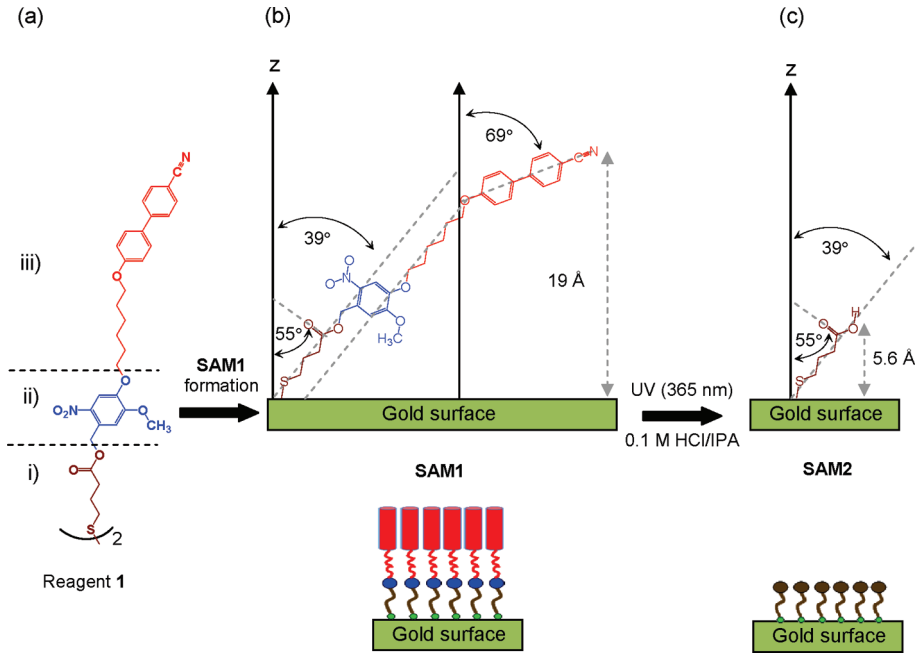

FIGURE 1. Schematic showing the structure of reagent 1 (a) and its possible orientation within SAMs of this compound (b) as formed and (c) after photocleavage based on ellipsometric and FTIR-reflectance studies (see below). Reagent 1 comprises (i) a surface binding group with protected-COOH unit (brown color); (ii) a photocleavable group (blue color); and (iii) liquid crystal analogue head group (red color). Reagent 1 forms SAM1 on gold and can be photocleaved under soft UV irradiation to reveal the −COOH functionalized SAM2.

Scheme 1. Synthesis of Reagent 1[a]

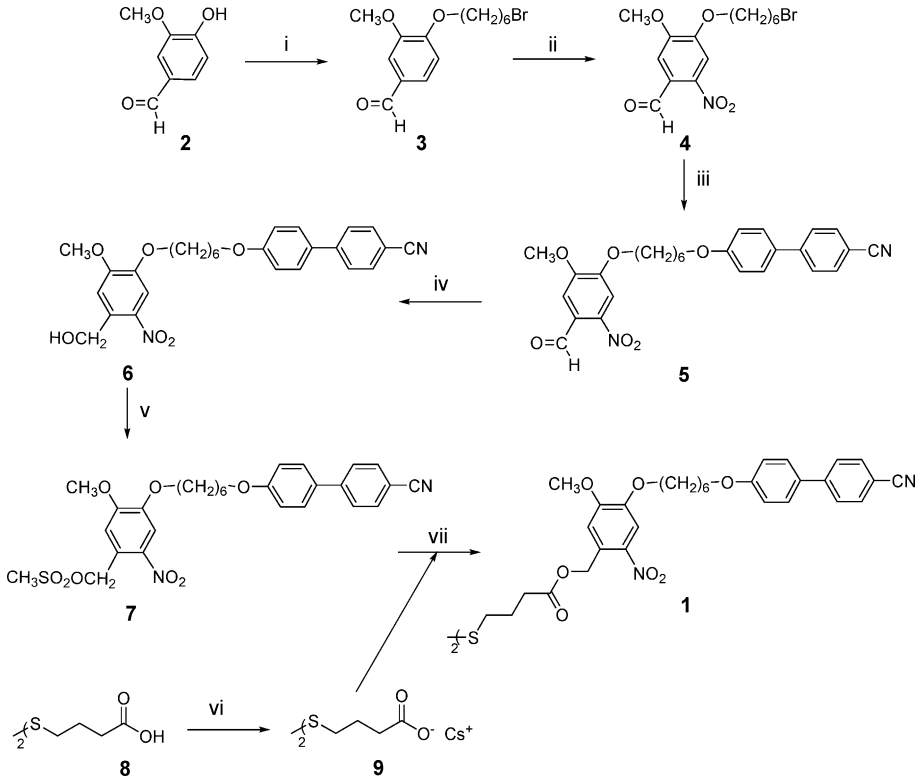

[a] Reagents and conditions. (i) Anhydrous K_2CO_3, DMF, $Br(CH_2)_6Br$, 60%; (ii) HNO_3, 79%; (iii) 4-hydroxy cyanobiphenyl, K_2CO_3, DMF, 87%; (iv) $NaBH_4$, THF, 74%; (v) CH_3SO_2Cl, TEA, THF, 87%; (vi) Cs_2CO_3, CH_3OH, 5 h; (vii) $-[S(CH_2)_3CO_2Cs]_2$, DMF, 76%.

Synthesis. Reagent **1** was designed to combine three functional segments as shown in Figure 1. Full details of synthesis and characterization are in the Supporting Information. The synthesis is outlined in Scheme 1. Vaniline was treated with a 4-fold excess of 1,6-dibromohexane under Williamson's ether synthesis conditions in the presence of mild base to yield monobromo compound **3** in 60% yield. This monobromo compound was nitrated using nitric acid to obtain the nitro derivative as reported previously (34). This nitro compound **4** was further treated with 4-hydroxy-4-cyanobiphenyl under Williamson's ether synthesis conditions to yield the compound **5** in good yield. The aldehyde functionality of compound **5** was

Table 1. Surface Properties of SAM1 and DTBA SAMs before and after Soft UV Irradiation

SAMs	water contact angles/degrees θ_{static}	$\theta_{advancing}$	$\theta_{receding}$	ellipsometric thickness/Å	expected thickness[c]/Å
fresh **SAM1**	75 ± 4	84 ± 1	52 ± 3	19 ± 2	19 (25)
SAM1 + UV[a] for 5 min	63 ± 4	70 ± 3	20 ± 2	6 ± 1	>5.6 (7.2)
SAM1 + UV[b] for 15 min	69 ± 4	75 ± 3	22 ± 2	7 ± 1	>5.6 (7.2)
fresh DTBA	<5	<5	<5	6 ± 1	5.6 (7.2)
DTBA + UV for 15 min	71 ± 3	80 ± 2	19 ± 3	5 ± 1	5.6 (7.2)

[a] 365 nm, dosage = 12 J cm^{-2}. [b] 365 nm, dosage = 36 J cm^{-2}. [c] Expected thickness of SAM using the length of a single molecule estimated from molecular modeling (HyperChem program, semi-empirical (AM1); values given in brackets) and assuming a tilt angle of 39° with respect to the surface normal.

reduced to the alcohol by sodium borohydride to obtain compound **6**. Compound **6** was treated with methane sulfonyl chloride in the presence of triethylamine to obtain the mesylate **7**. This mesylate ester was treated with the cesium salt of dithiobutyric acid **9** to obtain the reagent **1** (36).

Substrate Preparation. Glass microscope slides were cleaned by ultrasonication for 15 min in a 10% solution of Decon90 in Milli-Q water followed by a thorough rinsing in Milli-Q water and then dried under a stream of nitrogen. The slides were ultrasonicated in dichloromethane for 15 min, removed, and dried in a stream of zero grade nitrogen, rinsed under Milli-Q water, and immersed in piranha solution (70:30, v/v, H_2SO_4/H_2O_2) for 10 min. The substrates were then rinsed in Milli-Q water, dried under nitrogen, and placed in an Edwards Auto 306 thermal evaporator. A 150 nm gold layer was thermally deposited (at a rate of 0.1 nm s^{-1}) onto a chromium adhesion layer (5 nm thick), at a base pressure of approximately 1×10^{-6} mbar. The gold-coated samples were cleaned immediately prior to use by placing them in freshly prepared piranha solution for 2 min, followed by a rinse with Milli-Q water.

SAM Adsorption. Reagent **1** and DTBA SAMs were formed by immersing the gold-coated slides in 0.5 mM solutions of the corresponding material, in DCM, for 16 h, at 23 °C. The samples were then removed from solution, rinsed with DCM, dried with a nitrogen stream, rinsed with Milli-Q water, and again dried.

UV Irradiation. Soft UV (365 nm) light obtained from fluorescence microscope with a power (at sample) of 40 mW cm^{-2} was used to irradiate samples for wetting, ellipsometry, and X-ray photoelectron spectroscopy (XPS) studies and in the photo-patterning process. The UV light obtained from the microscope is controlled using UV pass filter which allows wavelength between 318 and 404 nm with the maximum transmission peak at 365 nm. A 365 nm UV lamp (Blak-Ray Model B100 AP) with a nominal power (at the sample) of 3.5 mW cm^{-2} for 2 h (25.2 J cm^{-2} UV dose) was used for only Fourier transform-infrared reflection absorption spectroscopy (FT-IRAS) studies to provide a larger illumination spot size. After the UV irradiation, samples were rinsed with DCM, followed by Milli-Q water, and finally dried under a stream of nitrogen.

Wetting Measurements. Contact angles were measured using a First-Ten-Angstrom 2000 goniometer under ambient conditions. Milli-Q water droplets were advanced and receded across the surface from a microsyringe needle. Images of at least five advancing and receding droplets were analyzed on both sides of each droplet to give a minimum of five values per surface.

X-ray Photoelectron Spectroscopy. XPS spectra were obtained using a Thermo Electron Corporation ESCA Lab 250 with a chamber pressure maintained below 1×10^{-9} mbar during acquisition. A monochromated Al Kα X-ray source (15 kV, 150 W) irradiated the samples, with a spot diameter of approximately 0.5 mm. The spectrometer was operated in Large Area XL magnetic lens mode using pass energies of 150 and 20 eV for survey and detailed scans, respectively. The spectra were obtained with an electron takeoff angle of 90°. High resolution spectra were fitted using the Avantage (Thermo VG software package) peak fitting algorithms. All spectra have been corrected such that the C 1s peak occurs at 284.5 eV to account for small variations in surface charging.

Fourier Transform-Infrared Reflection Absorption Spectroscopy. FT-IRAS spectra were obtained using a Bruker IFS-66 spectrometer equipped with a liquid nitrogen cooled MCT detector. The optical path was evacuated. A p-polarized beam at an incident angle of 80° to the surface normal was used for the Fourier transform infrared spectroscopy (FTIR) measurements. The spectra were taken at a 2 cm^{-1} resolution, and 1000 interferograms were co-added to yield spectra of high signal-to-noise ratio. The reference spectrum was taken from a freshly cleaned gold surface.

Ellipsometry. A Jobin-Yvon UVISEL spectroscopic ellipsometer was used to measure the thickness of the SAMs. The wavelength was varied between 300 and 800 nm, in steps of 10 nm. DeltaPsi2 software was used to model and fit the acquired data assuming a simple three-layer system. Values for the base layer (gold support) were obtained from a freshly cleaned gold substrate. The SAM was modeled as a transparent thin film using the Cauchy approximation, $n(\lambda) = A + B \times 10^4/\lambda^2 + C \times 10^9/\lambda^4$ and $k(\lambda) = 0$, where λ is the wavelength in units of nanometers and A, B, and C are the Cauchy parameters dependent on optical properties of the material. Parameter A was restricted to a value of 1.45, and parameters B and C were allowed to vary between 0 and 1 nm^2 and 0 and 0.2 nm, respectively. The ambient air was assumed to have $n = 1$ and $k = 0$. At least six ellipsometric measurements were made per sample on two or more samples of each type.

Liquid Crystals Studies. LC cells were constructed with CF_3 terminated SAMs, a homeotropic aligning surface, as the upper surface, and with a patterned **SAM1** lower surface. Cell thicknesses of 23 μm were achieved using thin strips of polyethylene terephthalate (PET) film (Goodfellow, UK). The samples were heated above the nematic−isotropic transition temperature of the LC to be investigated, and a small amount of LC was placed on the patterned surface before the upper surface was placed on top. The samples were then slowly cooled (0.1 °C min^{-1}) into the nematic and smectic phase and viewed under a polarizing microscope.

3. RESULTS AND DISCUSSION

Table 1 describes the surface properties of **SAM1** before and after photolysis using soft UV (365 nm), in 0.1 M HCl/isopropanol solution. The static contact angle (θ_{static}) of fresh **SAM1** is in agreement with the results observed for SAMs containing a cyano group conjugated by biphenyl and terphenyl rings (22). The large water contact angle hysteresis ($\theta_{advancing} - \theta_{receding} = 32°$) on the surface is likely due to increased disorder and chemical heterogeneity. Post UV irradiation, the advancing contact angle of **SAM1** (75° ± 3°),

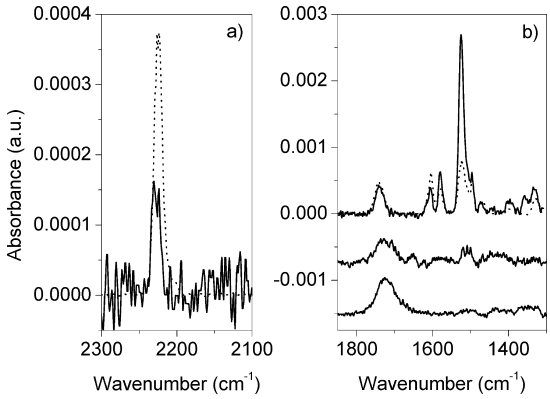

FIGURE 2. (a) FT-IRAS spectra of fresh SAM1 obtained from experimental observation (solid black line) and isotropic calculation for thin film of thickness 19 Å (dashed line). (b) FT-IRAS spectra of SAMs. Fresh SAM1 (upper trace solid), estimate from isotropic calculation (upper trace dashed), SAM1 irradiated in 0.1 M HCl/isopropanol with soft UV dosage of 25.2 J cm^{-2} (middle trace); and fresh DTBA SAM (lower trace).

approached, within error, that obtained from DTBA SAM after treatment in the same way (80° ± 2°). The higher advancing contact angles of photocleaved **SAM1** and irradiated DTBA compared to fresh carboxylic acid SAMs are most likely caused by the adsorption of adventitious contamination and possibly re-organization of monolayer in the case of **SAM1**. This leads to larger hysteresis of **SAM1** (53°) and DTBA (61°) after UV exposure. We note that root mean square (rms) surface roughness is 2 nm both before and after irradiation and is, therefore, not a major source of the hysteresis. The ellipsometrically determined SAM thickness of 19 ± 2 Å indicates that the average molecular tilt from surface normal is significant. The over-simplistic diagram in Figure 1 shows a molecular configuration consistent with the determined ellipsometric thickness, in which the alkyl groups are tilted ~39° and the cyano functionalized mesogenic groups are tilted ~69° with respect to the surface normal. A possible reason for large tilt angle of this cyano-biphenyl group is the minimization of electrostatic interaction between CN groups, which has been observed in thiol SAMs by Frey et al. on both Au and Ag surfaces (38).

The molecules used to form **SAM1** have distinctive vibrational modes between 2300 and 2200 cm^{-1} for the cyano group and 1600 and 1800 cm^{-1} for the phenyl and carbonyl vibrations, which in principle make it possible to estimate the orientational arrangement of these groups and possibly to infer something about the molecular arrangement. Figure 2a shows the experimentally obtained SAM spectrum together with that calculated from the KBr spectrum of the bulk material for an isotropic film of thickness 19 Å (39−42). The tilt angle of the C≡N stretching mode (~2229 cm^{-1}) (22, 24, 43−46) can be estimated from comparison of the observed and calculated spectra ($I_{obs}/3I_{calc} = \cos^2\theta$) which gives a tilt angle of 69° ± 2° which is in good agreement with the value found on the basis of the ellipsometry. Similar analysis of the C═O vibration (~1742 cm^{-1}) (36, 42, 47) indicates bond orientation of 54.7° with respect to the surface normal which also compares well with the model shown in Figure 1. Unfortunately, the overlap of absorption

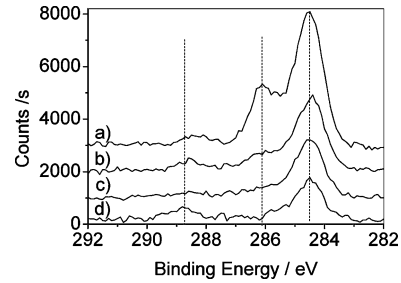

FIGURE 3. X-ray photoelectron spectra of the C 1s region. (a) Fresh SAM1 on Au; (b) SAM1 after 5 min UV dosage (12 J cm^{-2}); (c) SAM1 after 15 min (36 J cm^{-2}); and (d) fresh DTBA SAM. The dashed lines indicate the position of the Pseudo-Voigt peak functions (FHWM = 1.2 eV and a Lorenzian to Gaussian mix of 3:7) employed to fit the spectra.

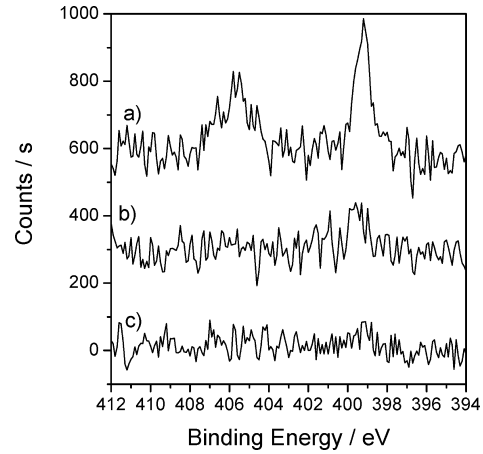

FIGURE 4. X-ray photoelectron spectra of the N 1s region. (a) Fresh SAM1 on Au; (b) SAM1 after 5 min of UV exposure (dosage 12 J cm^{-2}); and (c) SAM1 after 15 min of UV exposure (dosage, 36 J cm^{-2}).

bands in the region between ~1600 and 1000 cm^{-1} make it difficult to use these to obtain information regarding orientation. The peaks at 1606 and 1497 cm^{-1} correspond to C−C stretching of phenyl rings (44, 46, 48). The strong band at 1525 cm^{-1} and the weaker one between 1358 and 1335 cm^{-1} are associated with the asymmetric and symmetric stretching modes of aromatic NO_2 group, respectively (36, 49). Below 1300 cm^{-1}, there are numerous bands associated with the photocleavable unit and hydrocarbon backbone.

After soft UV exposure (Figure 2b; 25.2 J cm^{-2}), the peaks associated with the photo-removable moieties almost disappear leaving only the band at 1745 cm^{-1}, which is associated to the stretching mode of carboxylic acid terminal groups of SAM product and which is similar to the spectrum obtained for SAMs of DTBA (Figure 2b, lower trace). Following irradiation, the ellipsometric thicknesses of **SAM1** decreased substantially (Table 1) and approached the expected thickness (~5.6 Å).

X-ray photoelectron spectra of the C 1s region of **SAM1** on Au before and after photolysis are shown in Figure 3. The peaks located at 288.6 and 286.0 eV are related to the C═O groups (36, 50, 51) and C≡N and C−O species (37, 38, 45, 52, 53), respectively. The band at 284.5 eV is associated with the hydrocarbons CH_2 and CH_{arom} (36, 51, 52).

Table 2. Ratio of the XPS Peak Areas of the C 1s, N 1s, and O 1s Spectra to That of the Au 4f Peak of SAMs before and after Soft UV Irradiation[a]

	peak area/peak area Au 4f [normalized, %]		
SAMs on Au	C 1s	N 1s	O 1s
fresh **SAM1**	0.055 [100]	0.009 [100]	0.031 [100]
SAM1 + UV for 5 min	0.033 [60]	0.001 [10]	0.018 [58]
SAM1 + UV for 15 min	0.025 [45]	0.0005 [6]	0.010 [34]
DTBA + UV for 15 min	0.016 [30]	0.000 [0]	0.016 [52]
fresh DTBA	0.016 [30]	0.000 [0]	0.015 [48]

[a] The numbers in brackets are normalized to the **SAM1** values.

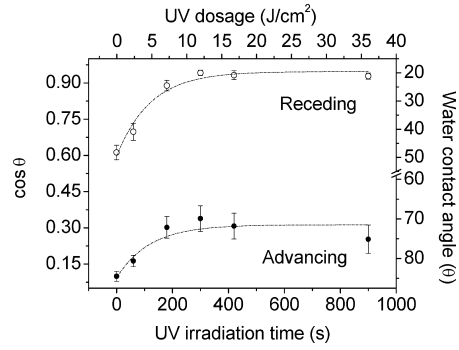

FIGURE 5. Variation of the advancing and receding water contact angles of SAM1 as a function of soft UV irradiation time under 0.1 M HCl/IPA, where θ represents the advancing or receding contact angles.

After soft UV deprotection for 5 and 15 minutes (Figure 3b,c), the main C peaks decrease and the spectrum approaches that of the DTBA SAM (Figure 3d). However, some residue of the starting material or some noncarboxyl product is also observed, at 286.0 eV, possibly formed from the acid radical. The broad weak peak at 288.6 eV is due to the C═O species (37).

Figure 4 shows the XPS data for the N 1s region. The two peaks, at 405.6 and 399.2 eV, correspond to the $-NO_2$ and −CN species, respectively (45, 51, 52, 54), and both of which are removed by exposure to soft UV. The peak areas obtained from XPS of SAMs in the C 1s and O 1s regions show reductions of 55% and 66%, respectively, following photolysis for 15 minutes (Table 2) whilst the N 1s peak is nearly completely removed (94 ± 2%). These changes are equivalent to a photoreaction yield of >90%, in agreement with our previous results on *ortho*-nitrobenzyl-protected carboxylic-based SAMs (37). We also note that the normalized peak areas of the C 1s and O 1s, with respect to Au 4f, of the DTBA SAM do not change during exposure to soft UV for 15 min, confirming that no degradation of the monolayer occurs during the photolysis process.

The advancing and receding water contact angles were measured as a function of UV exposure time and are shown in Figure 5. It was found that the cosine of the water contact angles increased monotonically with UV dosage plateauing after 400 s, equivalent to a UV dosage of 36 J cm^{-2}. The UV dosage required for achieving a high photolysis yield of **SAM1** (∼94%) was similar to that found for the *ortho*-nitrobenzyl-protected carboxylic acid-based SAMs reported previously (25.2 J cm^{-2}) (37).

The patterned SAM contains two different chemical functionalities, the cyanobiphenyl moiety oriented to promote homeotropic anchoring and the photocleaved carboxylic acid that promotes planar anchoring. The liquid crystal 8CB has a nematic phase between 34 and 39 °C and a smectic-A phase between 22 and 32 °C (55). Following patterning (with 12 J cm^{-2}), the sample was placed in a 0.5 mM DTBA SAM solution, in DCM, for 2 h to increase the surface energy in the photolysed region. This post-treatment was found to enhance the stability of the LC patterning for multiple cycles between the isotropic and smectic phases. Figure 6a−f shows 8CB in the smectic-A phase for stripes of different widths, on the same sample, confirming the effectiveness of photolysis of **SAM1** under soft UV (365 nm) irradiation and the ability of the resulting patterned SAM to control LC anchoring. When stripe sizes are varied, the formation of focal conic domains (FCDs), in the smectic-A phase, can be studied.

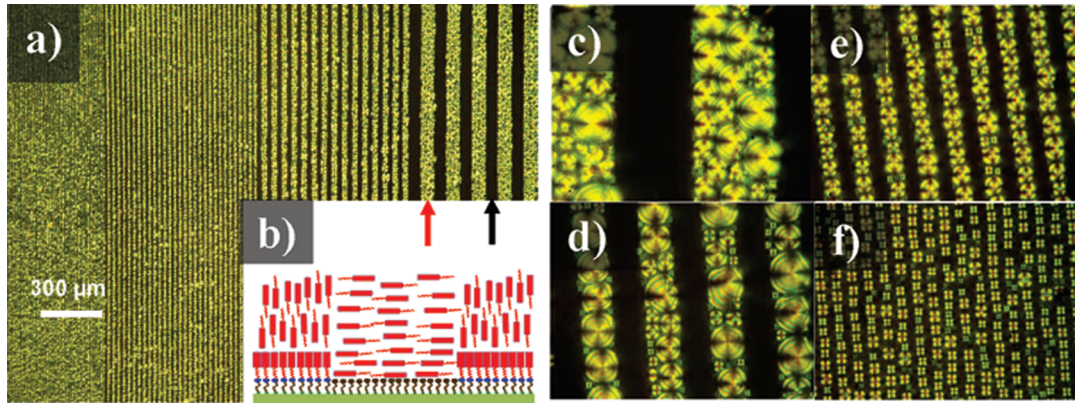

FIGURE 6. 8CB liquid crystal alignment on photopatterned SAM1 fabricated under soft UV (365 nm, 12 J cm^{-2}) followed by backfilling with 0.5 mM DTBA in DCM solution for 2 h. These images were taken using a polarizing microscope in the smectic-A phase ($T = 25$ °C). (a) Shows a pattern containing stripes of varying width. (b) Shows the alignment of 8CB liquid crystals on the photopatterned SAM1. The red and black arrows point to planar alignment on photocleaved and homeotropic alignment on nonreacted SAM1 regions, respectively. The red rods represent the cyano-biphenyl group in SAM1 and 8CB molecules in the bulk phase. (c−f) Show stripes of different periodicity: (c) 50 μm, (d) 20 μm, (e) 10 μm, and (f) 5 μm.

The FCDs observed here represent the case in which the ellipticity of the domains are close to zero. The defects are known as toroidal focal conic domains (TFCDs) (56). When confined in a LC cell, if the lower surface promotes planar alignment and the top surface promotes homeotropic alignment, FCDs form so that the smectic layers curve to match the antagonist boundary conditions. Multiple FCDs of different sizes form inside cells and tile the space to form a matrix of defects. The FCDs obey Freidels laws of association, which state that the FCDs are in tangential contact with each other (56). For a given anchoring energy, for a particular LC, on the top and bottom surfaces, and for a set cell thickness, there is a minimum in the free energy that determines the size of FCDs observed (57−59). When the surface is patterned on a scale smaller than this, the patterning geometry determines the size and position of the FCDs. Previous studies have shown that microcontact printed patterned SAMs (29) and other patterned surfaces (60) can be used in this way to control FCDs. Here, we show that a novel photo-patternable SAM can also be used. In particular, it was found that the size of FCD could be confined by the stripe width. The large stripes with widths of 50 and 20 μm allow multiple FCDs to form whereas small stripes with widths of 10 and 5 μm could effectively control 8CB molecules to form a single FCD across stripe the width. Such control over FCD behavior is of interest (60, 61) for potential applications in photonics (10) or as templates to control self-assembly of micro- and nanosystems (62).

4. CONCLUSIONS

A novel cyano-biphenyl-based thiol containing a photocleavable group was shown to form self-assembled monolayers on gold surfaces. Photolysis of the cyanobiphenyl moiety, using soft UV, led to the production of a carboxylic acid rich surface with a high reaction yield (>90%). Such binary patterned surfaces can be used to control the alignment of overlying LC phases and the positioning of FCD defects. The approach has the advantage of requiring fewer steps to control the formation of FCDs, in terms of positioning and size confinement on surfaces. Further, complex geometries can be explored which are not accessible with more traditional routes for controlling LC alignment. Finally, the small stripes with width of 10 μm or less were shown to control effectively the LC molecules such that a single FCD across the stripe was formed.

Acknowledgment. We would like to thank Royal Thai Government for the provision of a PhD scholarship. We acknowledge the support by the RCUK's Basic Technology Research programme.

Supporting Information Available: Full details of synthesis and characterization of the Reagent **1**. This material is available free of charge via the Internet at http://pubs.acs.org.

REFERENCES AND NOTES

(1) Schadt, M. *Annu. Rev. Mater. Sci.* **1997**, *27*, 305–379.
(2) Tannas, L. E.; Glenn, W. E.; Doane, J. W. *Flat-Panel Display Technologies—Japan, Russia, Ukraine, and Belarus*; Noyes Publications: Park Ridge, N.J., 1995.
(3) Collings, P. J. *Liquid crystals: nature's delicate phase of matter*, 2nd ed.; Princeton University Press: Princeton, N.J.; Oxford, 2002.
(4) Sridharamurthy, S. S.; Cadwell, K. D.; Abbott, N. L.; Jiang, H. *Smart Mater. Struct.* **2008**, *17*, 1–4.
(5) Brake, J. M.; Daschner, M. K.; Luk, Y. Y.; Abbott, N. L. *Science* **2003**, *302*, 2094–2097.
(6) Shah, R. R.; Abbott, N. L. *Langmuir* **2003**, *19*, 275–284.
(7) Hussain, A.; Pina, A. S.; Roque, A. C. A. *Biosens. Bioelectron.* **2009**, *25*, 1–8.
(8) Alkeskjold, T. T.; Scolari, L.; Noordegraaf, D.; Laegsgaard, J.; Weirich, J.; Wei, L.; Tartarini, G.; Bassi, P.; Gauza, S.; Wu, S. T.; Bjarklev, A. *Opt. Quantum Electron.* **2007**, *39*, 1009–1019.
(9) Wei, L.; Weirich, J.; Alkeskjold, T. T.; Bjarklev, A. *Opt. Lett.* **2009**, *34*, 3818–3820.
(10) Ruan, L. Z.; Sambles, J. R.; Stewart, I. W. *Phys. Rev. Lett.* **2003**, *91*, 033901.
(11) O'Neill, M.; Kelly, S. M. *J. Phys. D: Appl. Phys.* **2000**, *33*, R67–R84.
(12) Geary, J. M.; Goodby, J. W.; Kmetz, A. R.; Patel, J. S. *J. Appl. Phys.* **1987**, *62*, 4100–4108.
(13) Janning, J. L. *Appl. Phys. Lett.* **1972**, *21*, 173–174.
(14) Drawhorn, R. A.; Abbott, N. L. *J. Chem. Phys.* **1995**, *99*, 16511–16515.
(15) Cheng, Y. L.; Batchelder, D. N.; Evans, S. D.; Henderson, J. R.; Lydon, J. E.; Ogier, S. D. *Liq. Cryst.* **2000**, *27*, 1267–1275.
(16) Bramble, J. P.; Evans, S. D.; Henderson, J. R.; Anquetil, C.; Cleaver, D. J.; Smith, N. J. *Liq. Cryst.* **2007**, *34*, 1059–1069.
(17) Cadwell, K. D.; Lockwood, N. A.; Nellis, B. A.; Alf, M. E.; Willis, C. R.; Abbott, N. L. *Sens. Actuators, B* **2007**, *128*, 91–98.
(18) Evans, S. D.; Allinson, H.; Boden, N.; Henderson, J. R. *Faraday Discuss.* **1996**, *104*, 37–48.
(19) Evans, S. D.; Allinson, H.; Boden, N.; Flynn, T. M.; Henderson, J. R. *J. Phys. Chem. B* **1997**, *101*, 2143–2148.
(20) Alkhairalla, B.; Allinson, H.; Boden, N.; Evans, S. D.; Henderson, J. R. *Phys. Rev. E: Stat., Nonlinear, Soft Matter Phys.* **1999**, *59*, 3033–3039.
(21) Alkhairalla, B.; Boden, N.; Cheadle, E.; Evans, S. D.; Henderson, J. R.; Fukushima, H.; Miyashita, S.; Schonherr, H.; Vancso, G. J.; Colorado, R.; Graupe, M.; Shmakova, O. E.; Lee, T. R. *Europhys. Lett.* **2002**, *59*, 410–416.
(22) Critchley, K.; Cheadle, E. M.; Zhang, H. L.; Baldwin, K. J.; Liu, Q. Y.; Cheng, Y. L.; Fukushima, H.; Tamaki, T.; Batchelder, D. N.; Bushby, R. J.; Evans, S. D. *J. Phys. Chem. B* **2009**, *113*, 15550–15557.
(23) Agarwal, A. K.; Suresh, K. A.; Pal, S. K.; Kumar, S. *J. Chem. Phys.* **2007**, *126*, 164901.
(24) Zhang, H. L.; Evans, S. D.; Critchley, K.; Fukushima, H.; Tamaki, T.; Fournier, F.; Zheng, W.; Carrez, S.; Dubost, H.; Bourguignon, B. *J. Chem. Phys.* **2005**, *122*, 224707.
(25) Boden, N.; Bushby, R. J.; Martin, P. S.; Evans, S. D.; Owens, R. W.; Smith, D. A. *Langmuir* **1999**, *15*, 3790–3797.
(26) Fukushima, H.; Tamaki, T. *J. Phys. Chem. B* **2002**, *106*, 7142–7145.
(27) Ganesh, V.; Pal, S. K.; Kumar, S.; Lakshminarayanan, V. *Electrochim. Acta* **2007**, *52*, 2987–2997.
(28) Malone, S. M.; Schwartz, D. K. *Langmuir* **2008**, *24*, 9790–9794.
(29) Bramble, J. P.; Evans, S. D.; Henderson, J. R.; Atherton, T. J.; Smith, N. J. *Liq. Cryst.* **2007**, *34*, 1137–1143.
(30) Gupta, V. K.; Abbott, N. L. *Science* **1997**, *276*, 1533–1536.
(31) Lee, B. W.; Clark, N. A. *Science* **2001**, *291*, 2576–2580.
(32) Fukushima, H.; Takiguchi, H.; Shimoda, T.; Masuda, T.; Bushby, R. J.; Evans, S.; Jeyadevan, J. P.; Critchley, K. UV decomposable molecules and a photopatternable monomolecular film formed therefrom. US2005245739 (A1); November 3, 2005.
(33) Nakagawa, M.; Ichimura, K. *Colloids Surf., A: Physicochem. Eng. Aspects* **2002**, *204*, PII S0927-7757(01)01002-0.
(34) Critchley, K.; Jeyadevan, J. P.; Fukushima, H.; Ishida, M.; Shimoda, T.; Bushby, R. J.; Evans, S. D. *Langmuir* **2005**, *21*, 4554–4561.
(35) Besson, E.; Gue, A. M.; Sudor, J.; Korri-Youssoufi, H.; Jaffrezic, N.; Tardy, J. *Langmuir* **2006**, *22*, 8346–8352.
(36) Critchley, K.; Zhang, L. X.; Fukushima, H.; Ishida, M.; Shimoda, T.; Bushby, R. J.; Evans, S. D. *J. Phys. Chem. B* **2006**, *110*, 17167–17174.
(37) Prompinit, P.; Achalkumar, A. S.; Han, X. J.; Bushby, R. J.; Walti, C.; Evans, S. D. *J. Phys. Chem. C* **2009**, *113*, 21642–21647.

(38) Frey, S.; Shaporenko, A.; Zharnikov, M.; Harder, P.; Allara, D. L. *J. Phys. Chem. B* **2003**, *107*, 7716–7725.
(39) Allara, D. L.; Swalen, J. D. *J. Chem. Phys.* **1982**, *86*, 2700–2704.
(40) Allara, D. L.; Nuzzo, R. G. *Langmuir* **1985**, *1*, 52–66.
(41) Evans, S. D.; Urankar, E.; Ulman, A.; Ferris, N. *J. Am. Chem. Soc.* **1991**, *113*, 4121–4131.
(42) Nuzzo, R. G.; Dubois, L. H.; Allara, D. L. *J. Am. Chem. Soc.* **1990**, *112*, 558–569.
(43) de Bleijser, J.; Leyte-Zuiderweg, L. H.; Leyte, J. C.; van Woerkom, P. C. M.; Picken, S. *J. Appl. Spectrosc.* **1996**, *50*, 167–173.
(44) Nakano, T.; Yokoyama, T.; Toriumi, H. *Appl. Spectrosc.* **1993**, *47*, 1354–1366.
(45) Sato, Y.; Ye, S.; Haba, T.; Uosaki, K. *Langmuir* **1996**, *12*, 2726–2736.
(46) Toriumi, H.; Sugisawa, H.; Watanabe, H. *Jpn. J. Appl. Phys., Part 2* **1988**, *27*, L935–L937.
(47) Duevel, R. V.; Corn, R. M. *Anal. Chem.* **1992**, *64*, 337–342.
(48) Akiyama, H.; Tamada, K.; Nagasawa, J.; Abe, K.; Tamaki, T. *J. Phys. Chem. B* **2003**, *107*, 130–135.
(49) Nakanishi, K. *Infrared absorption spectroscopy, practical*; Nankodo Company Limited: Tokyo, 1962.
(50) Ok, C. H.; Kim, B. Y.; Oh, B. Y.; Kim, Y. H.; Lee, K. M.; Park, H. G.; Han, J. M.; Seo, D. S.; Lee, D. K.; Hwang, J. Y. *Liq. Cryst.* **2008**, *35*, 1373–1377.
(51) Beamson, G. *High Resolution XPS of Organic Polymers The Scienta ESCA300 Database*; Wiley: Chichester, UK, 1992.
(52) Artyushkova, K.; Fulghum, J. E.; Reznikov, Y. *Mol. Cryst. Liq. Cryst.* **2005**, *438*, 1769–1777.
(53) Bain, C. D.; Troughton, E. B.; Tao, Y. T.; Evall, J.; Whitesides, G. M.; Nuzzo, R. G. *J. Am. Chem. Soc.* **1989**, *111*, 321–335.
(54) Moulder, J. F.; Stickle, W. F.; Sobol, P. E.; Bomben, K. D. *Handbook of X-ray Photoelectron Spectroscopy: A Reference Book of Standard Spectra for Identification of XPS Data*; Physical Electronics, Inc.: Chanhassen, Minnesota, 1995.
(55) Morsy, M. A.; Oweimreen, G. A.; Hwang, J. S. *J. Chem. Phys.* **1996**, *100*, 8331–8337.
(56) Kleman, M.; Lavrentovich, O. *Soft Matter Physics*; Springer: New York, 2003.
(57) Blanc, C.; Kleman, M. *Eur. Phys. J. B* **1999**, *10*, 53–60.
(58) Blanc, C.; Kleman, M. *Phys. Rev. E: Stat., Nonlinear, Soft Matter Phys.* **2000**, *62*, 6739–6748.
(59) Fournier, J. B.; Dozov, I.; Durand, G. *Phys. Rev. A* **1990**, *41*, 2252–2255.
(60) Guo, W.; Herminghaus, S.; Bahr, C. *Langmuir* **2008**, *24*, 8174–8180.
(61) Choi, M. C.; Pfohl, T.; Wen, Z. Y.; Li, Y. L.; Kim, M. W.; Israelachvili, J. N.; Safinya, C. R. *Proc. Nat. Acad. Sci. U.S.A.* **2004**, *101*, 17340–17344.
(62) Yoon, D. K.; Choi, M. C.; Kim, Y. H.; Kim, M. W.; Lavrentovich, O. D.; Jung, H. T. *Nat. Mater.* **2007**, *6*, 866–870.

AM100832P